PHYSICAL REVIEW B **80**, 075426 (2009)

Photoluminescence spectral imaging of ultralong single-walled carbon nanotubes: Micromanipulation-induced strain, rupture, and determination of handedness

Oliver Kiowski,[1,2] Stefan-Sven Jester,[1] Sergei Lebedkin,[1,*,†] Zhong Jin,[3] Yan Li,[3] and Manfred M. Kappes[1,2,*,‡]
[1]*Institut für Nanotechnologie, Forschungszentrum Karlsruhe, D-76021 Karlsruhe, Germany*
[2]*Institut für Physikalische Chemie, Universität Karlsruhe, D-76128 Karlsruhe, Germany*
[3]*Beijing National Laboratory for Molecular Sciences, Key Laboratory of Physics and Chemistry of Nanodevices, College of Chemistry and Molecular Engineering, Peking University, Beijing 100871, China*

(Received 15 April 2009; revised manuscript received 16 July 2009; published 20 August 2009)

We have applied photoluminescence (PL) microscopy with scanning laser excitation wavelength for imaging and characterizing individual, millimeter-long, single-walled carbon nanotubes (SWNTs) grown by chemical-vapor deposition on structured Si/SiO_2 substrates. Trenches etched into the substrates allowed a direct comparison of the PL properties of air-suspended (across the trenches) and on-SiO_2 segments of the same semiconducting nanotubes. For the on-SiO_2 segments, we found an ~10–20-fold decrease in PL intensity and redshifts of the emission and excitation transitions by 7–27 meV and 5–24 meV, respectively, compared to air-suspended regions of the same SWNTs. Furthermore, PL imaging was applied to SWNTs fractured by dragging an atomic force microscope tip across on-SiO_2 segments. Strong, localized changes in the emission properties were observed. These included the appearance of PL blinking at the fracture site and evidence for residual axial and to a lesser extent torsional strain extending tens of microns away from the fracture site. We also discuss how PL measurements of torsional strain can be used to determine the handedness of a luminescent nanotube.

DOI: 10.1103/PhysRevB.80.075426 PACS number(s): 78.67.Ch, 78.55.−m, 81.07.De

I. INTRODUCTION

Recent progress in chemical-vapor deposition (CVD) growth of single-walled carbon nanotubes (SWNTs) has resulted in the production of arrays of aligned individual millimeter-long nanotubes grown horizontally on Si/SiO_2 substrates in a regular and controlled fashion.[1,2] These nanotube configurations provide various options for electrical contacting and microstructuring the substrates and therefore would optimally suit many proposed SWNT devices such as chemical, biochemical, or electromechanical sensors. Ultralong SWNTs on microstructured substrates also open new experimental possibilities, for instance, for Raman studies of torsional and axial strain induced in nanotubes by atomic force microscopy (AFM) manipulation.[3,4] Near-infrared photoluminescence (PL) microscopy may be applied as a complimentary and versatile method to probe semiconducting (emitting) SWNTs in the above arrays. It allows determining nanotube structure (defined conventionally by two integer indices n,m) and is quite sensitive to nanotube surrounding, temperature, strain, and defects.[5–9] However, the majority of PL studies have so far been performed on surfactant- and polymer-coated SWNTs (either in dispersion or after deposition onto substrates by spin coating) as well as on free-standing, air-suspended segments of SWNTs. In such surroundings, the PL efficiency is relatively high. Quantum yields of up to a few percent have been estimated for air-suspended nanotubes.[10] This circumstance has particularly facilitated PL microscopy and imaging of single nanotubes.[8–12] In contrast, PL was initially considered to be immeasurably small for nanotubes in contact with a dielectric surface, e.g., for nanotubes grown horizontally on silicon wafers. Recently, we have shown that the emission of SWNTs on substrates such as sapphire and Si/SiO_2 is strongly reduced but not completely quenched. It can in fact be reliably detected with a PL laser microscope.[13,14]

In this contribution, we present a PL spectral imaging study of ultralong individual SWNTs grown by CVD on microstructured Si/SiO_2 substrates. Thus, we were able to directly compare PL in these two different local surroundings for the same nanotubes. To record characteristic shifts of the emission (E_{11}) and excitation (E_{22}) energies of SWNTs, emission spectra were acquired at each pixel of the sample scanned and, additionally, full PL maps (PL intensity vs excitation and emission wavelengths) were obtained at close sites along a specific nanotube fragment. Furthermore, such PL spectral imaging was applied to study the outcome of straining and fracturing SWNTs by moving a mechanically contacting AFM tip across on-SiO_2 tube segments at right angles to their cylinder axis. Strong changes in the PL spectra were observed at what appeared to be fracture sites. PL also reveals residual torsional and axial strain in such manipulated nanotubes. Micro-PL detection of torsional strain on both sides of the AFM tip-interaction region is especially interesting since it allows determining the handedness of individual luminescent (chiral) nanotubes.

II. EXPERIMENTS

Arrays of SWNTs were grown on silicon substrates covered with a 500-nm-thick oxide layer. This was done using an ultralow gas flow CVD process as described elsewhere.[2] Briefly, a Fe-Mo nanoparticle solution was applied to one end of the substrate. After drying, the substrate was heated to 900 °C in a hydrogen gas flow (100 sccm). Growth of SWNTs was subsequently carried out at 970 °C in a flow of methane (2 sccm) and hydrogen (4 sccm). The SWNTs produced were aligned roughly parallel to the gas flow direction

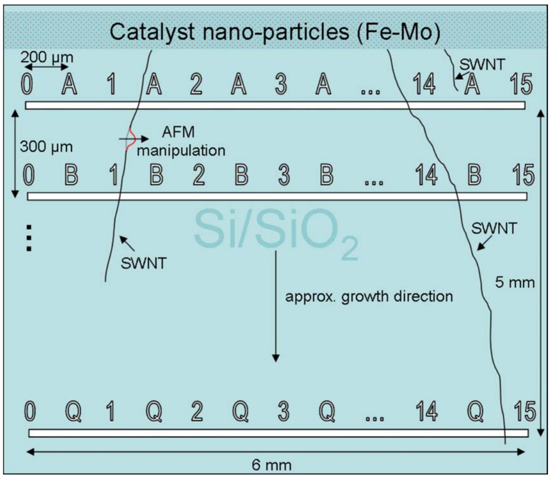

FIG. 1. (Color online) Schematic layout of a Si/SiO$_2$ substrate with 3.5-μm-wide and 0.5-μm-deep etched trenches (white horizontal stripes), etched markers (40 μm high letters and numbers) and three exemplary carbon nanotubes of different lengths grown by the catalytic CVD process. The length and geometry of these nanotubes on the substrate are depicted as determined by scanning electron microscopy. For instance, the longest depicted nanotube was found to have a length of about 6 mm and crossed 17 trenches. Manipulation with an atomic force microscope tip is illustrated for the left nanotube (after applying a drag force in contact mode perpendicular to the nanotube axis).

and had a length of up to several millimeters. The typical area density of SWNTs in these arrays was less than 1 μm^{-2}, which facilitated PL measurements on individual nanotubes. In order to produce air-suspended segments of nanotubes, 3.5-μm-wide and 500-nm-deep parallel trenches were lithographically etched on the substrate prior to tube growth. Trenches were separated from each other by 300 μm and oriented perpendicular to the growth direction. In addition, markers were etched to allow precise substrate positioning and retrieval of nanotubes. A schematic layout of a substrate with CVD-grown nanotubes is shown in Fig. 1. AFM analysis yielded an SWNT diameter distribution ranging from 0.9 to 3.3 nm with a mean value of 2 nm.[2] AFM manipulation was performed with a Veeco CPII as described elsewhere.[14,15] Nanotubes were mechanically stressed to fracture by applying a lateral drag force with an AFM tip (Mikromasch NSC18) at on-SiO$_2$ regions located between trenches on the substrate.

PL of individual nanotubes was measured with a home-built near-infrared confocal microscope using two separately tunable Ti:Sapphire cw lasers (Spectra Physics) to cover excitation wavelengths in the range of 695–1000 nm and an InGaAs photodiode array (Roper Scientific) for emission detection.[9,14] A near-infrared microscope objective (100x, NA=0.95) was applied to focus the excitation beam (typical excitation power of 1–2 mW, estimated power density of ~5–10 KW/cm^2) and to collect emission light. The substrate was positioned under the objective such that the laser beam polarization was roughly collinear with the nanotube growth direction (Fig. 1). To protect nanotubes from a possible oxidation via laser heating, the sample holder and the objective were enclosed and purged with a slow flow of the nitrogen or argon gas. The usable emission range was restricted to ~1200–1600 nm by the background luminescence of the Si/SiO$_2$ substrates and by the sensitivity of the detector (lower and upper wavelength limits, respectively). This range corresponds to SWNTs having diameters between approximately 1.0 and 1.4 nm. PL was detected for ~5% of nanotubes counted by scanning electron microscopy (SEM).[16] Such a small fraction is not surprising, given the pertaining Gaussian distribution of nanotube diameters centered at 2 nm [with full width at half maximum (FWHM) of 1.2 nm], in accordance with the aforementioned AFM results, and the statistical ratio (2:1) for semiconducting vs metallic (nonluminescent) SWNTs.

Emitting SWNTs were first identified by localizing PL signals along the trench next to the catalyst stripe (Fig. 1). For this, the sample was moved under the objective with the aid of a X-Y-Z-piezo/micrometer stage. Characteristic emission (E_{11}) and excitation (E_{22}) energies correlating with the nanotube (n,m) structure were then determined from a PL map such as that shown in Fig. S1,[15] acquired by scanning the laser excitation wavelength (typically in 1–3 nm steps) while keeping the piezo stage stationary. The typically single PL peak on such a map was fitted with a two-dimensional Lorentz function, also providing peak bandwidth [FWHM(E_{11}, E_{22})]. Positional tracking of the emitting nanotube on the substrate was then done either by PL probing at selected positions along the tube or by imaging whole areas. In the latter case, the sample was typically scanned in 0.2 μm steps in X and Y directions, resulting in a pixel size of 0.2×0.2 μm^2. A PL image was constructed by integrating the corresponding emission signals within a specific PL wavelength range for each pixel (WITEC Spectra Analyzer software). In the imaging mode, acquisition times were 1–10 s per spectrum or pixel. Four nanotubes with different (n,m) structures were also characterized by PL "spectral profiling," i.e., by acquiring a sequence of full PL maps in small increments along a nanotube segment. Two of these extensively characterized nanotubes were AFM manipulated (see below). In the following, we mainly describe results obtained for these four nanotubes numbered 1–4.

III. RESULTS AND DISCUSSION

Figure 2(a) shows a PL image of nanotube 3. This image is typical insofar as stable and uniform emission from both on-SiO$_2$ and air-suspended segments is observed. However, the former segments show ~10–20 times lower-emission intensity relative to the air-suspended counterparts. A similar reduction has been estimated for SWNTs on Si/SiO$_2$ and sapphire surfaces in previous work.[13,14] Correspondingly, air-suspended segments appear as short bright stripes across the trenches [Fig. 2(a)]. The latter typically appear darkly shadowed in PL images because of a smaller background signal from the out-of-focus trench bottom. The imaged nanotubes have an apparent width of ~400 nm, which corresponds to the lateral resolution of the near-infrared PL microscope. Note that PL signals, in particular, from air-suspended segments, showed a nonlinear dependence on the excitation power (between linear and square-root functions) at the

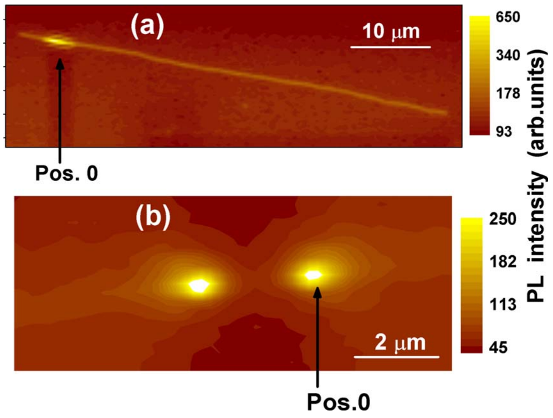

FIG. 2. (Color online) (a) PL image of partially luminescent nanotube 3 assigned to a noncontinuous (n,m) structure (i.e., change in chiral index at both left- and right-hand image perimeters, see text). The bright emission stripe in the upper left corner corresponds to a nanotube segment suspended over the trench (dark shadow). (b) Expanded PL image of a trench crossed by SWNT 2. The nanotube contacts the trench bottom in the middle resulting in strongly reduced PL. "Position 0" marks the starting point of PL profiles along these nanotubes as shown in Fig. 3 (from this point to the right).

power density of $\sim 5-10$ KW/cm^2 (see experiments). The nonlinearity can be attributed to a simultaneous generation of multiple excitons in a nanotube (with the onset at ~ 1 KW/cm^2 for air-suspended segments) and their nonradiative recombination.[17] Taking this effect into account, the ratio between PL signals of suspended and on-SiO_2 segments may increase by a factor of $\sim 2-3$, when extrapolated to the very low-excitation intensities. The exact mechanism of PL quenching by the Si/SiO_2 (or sapphire) surface is presently unclear. Theoretical studies have demonstrated a significant modulation of electronic properties of SWNTs in the nanotube-on-surface configuration, for instance, a dramatic effect of surface phonons of a polar dielectric substrate such as SiO_2 on the electron mobility in semiconducting nanotubes.[18,19] We suppose a similarly strong influence of the SiO_2 or Al_2O_3 surface on nonradiative relaxation of the electronic excitations (excitons) in SWNTs.

Figure 2(a) also shows abrupt transitions from a "bright" central to "dark" perimeter on-SiO_2 regions. This is a comparatively rare example of a *partially* luminescent long SWNT. According to SEM data and the sample layout (position of the catalyst), nanotube 3 extends in both directions by hundreds of micrometers relative to the image shown in Fig. 1(a). However, it does not luminesce outside of the area shown (as checked at selected sites using long acquisition times and elevated excitation power). We attribute the abrupt transitions between the bright and dark segments to changes in the (n,m) structure of this nanotube, which occurred during the CVD growth. The dark sections either correspond to metallic (nonluminescent) or to semiconducting regions emitting beyond our detection range. Examples of discontinuous changes in the (n,m) structure of a single SWNT have already been reported for CVD-grown nanotubes.[10,20] Nevertheless, the CVD process used in this work appears to normally produce SWNTs having uniform (n,m) structure over their entire length (up to a few millimeters). Indeed, no dark regions were observed for SWNTs 1, 2, and 4 probed over distances of up to 600 μm. Furthermore, the emission and excitation energies measured for these SWNTs could be assigned to one continuous (n,m) structure taking into account energy shifts induced by the surroundings (surface vs air suspension), as discussed below. Note that controlled growth of nanotubes having (n,m)-(n',m') junctions, e.g., metal-semiconductor transitions at selected positions would be of great interest. It is, however, not yet clear, which growth parameters provide such control.

Bright, uniform emission from air-suspended nanotube segments [Fig. 2(a)], was observed for the majority (seven out of nine) of trench crossings. This confirms that 3.5-μm-wide and 0.5-μm-deep trenches can be readily bridged in the ultralow gas flow CVD process, typically without touching the trench bottom. Nearly uniform PL was observed even for a ~ 30 μm long segment of SWNT 1 suspended accidentally over an etched marker. On the other hand, one trench crossing yielded the PL image shown in Fig. 2(b), with two bright PL spots close to the trench edges and a weak emission in between. This image can be attributed to $SWNT/SiO_2$ mechanical contact at the trench bottom, resulting in strongly reduced emission intensity at this site.

Figure 3 highlights quantitative differences in PL of air-suspended vs on-SiO_2 nanotube segments. Plotted are profiles of the emission intensity, $E_{11,22}$ energies, and bandwidths [FWHM($E_{11,22}$)] as obtained from PL maps measured in regular increments along the lengths of SWNTs 1–3. The profiles for nanotubes 1 and 2 start at a trench edge. For 1, the profiles also include the aforementioned ~ 30 μm long segment suspended over the etched marker (between positions ~ 240 and ~ 270 μm in Fig. 3). Besides the much weaker emission, the optical transitions are redshifted for on-SiO_2 vs air-suspended nanotube segments. Table I lists the averages of PL parameters as measured for air-suspended and on-SiO_2 segments of SWNTs 1–4 together with their (n,m) assignment. Redshifts of up to 27 and 24 meV were observed for the E_{11} and E_{22} energies, respectively.[21] They can be explained by the different extent of external dielectric screening of excitations (excitons) in SWNTs.[9,22–26] For on-SiO_2 segments, a first approximation of the effective dielectric constant, $\varepsilon_{\mathrm{eff}}$, is obtained by assuming that screening reflects a SiO_2 half space. Consequently, $\varepsilon_{\mathrm{eff}}$ can be taken as $\sim(\varepsilon_{\mathrm{air}}+\varepsilon_{\mathrm{SiO2}})/2=2.15$, where $\varepsilon_{\mathrm{air}}=1$ and $\varepsilon_{\mathrm{SiO2}}=3.3$ are the dielectric constants of air and SiO_2, respectively. Since the nanotubes only touch SiO_2, rather than being semiembedded, the actual value of $\varepsilon_{\mathrm{eff}}$ is likely lower than the above estimate. Indeed, SWNTs dispersed in water-surfactant and organic solutions ($\varepsilon_{\mathrm{eff}}\sim 2$) show approximately two times larger redshifts of E_{11} and E_{22} energies as compared to air-suspended nanotube segments.[9,24] In contrast to PL intensity and $E_{11,22}$ energies, we observed no clear effect of the substrate on PL bandwidths. The minor increase in FWHM(E_{11}) seen for the suspended part of SWNT 1 (Fig. 3) is likely a fitting artifact because this nanotube emits at a wavelength close to the detector cutoff.

We now discuss results for the AFM-manipulated SWNTs 1 and 2. Note that they belong to different $p=(n\text{-}m)\bmod 3$

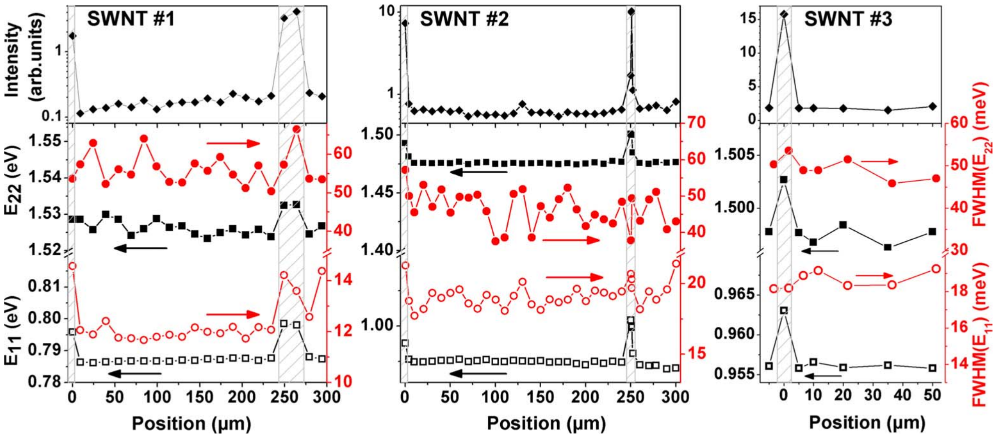

FIG. 3. (Color online) Profiles of PL peak energies E_{11} and E_{22}, bandwidths FWHM($E_{11,22}$), and relative intensities as measured along the length of nanotubes 1–3 grown by CVD on a Si/SiO$_2$ substrate. Hatched regions denote air-suspended nanotube segments (see text). The position axis corresponds to the X axis of the sample stage which essentially coincides with nanotube growth direction.

families (Table I). According to AFM and PL images (Fig. 4), the micromanipulation procedure yields nanotube segments pushed away from their original position over a length of ~1–2 μm and fractured at an excursion of ~0.3–0.5 μm from the starting point [corresponding to a lateral drag from left to right as seen in Figs. 1 and 4(a)]. Beyond this region, we imaged practically unchanged, straight SWNT sections. However, micro-Raman studies have shown that mechanical strain within such severely deformed nanotubes is still measurable tens of micrometers away from the manipulation point.[3,4] Although some strain relaxation is expected after removal of the AFM tip (and after a nanotube fracture), apparently significant residual strain may remain due to interactions ("friction") between nanotube and substrate. This is also evidenced by the micro-PL data (see below).

Figures 5 and S2 (Supplementary Information) (Ref. 15) show PL profiles around the fracture sites for SWNTs 1 and 2, respectively. Profiles acquired before AFM manipulation are also shown for comparison. Positive and negative positions on these plots correspond, respectively, to nanotube segments/fragments below and above the manipulation (fracture) point as seen in Figs. 1 and 4. At the fracture point (position 0), we find significant and highly localized changes in the PL (to within the ~400 nm spatial resolution). In particular, enhanced emission intensity and blueshifts of the $E_{11,22}$ energies are observed. Particularly strong changes were recorded for SWNT 1: a ~7-fold increase in the PL intensity and +62 and +85 meV shifts of E_{11} and E_{22}, respectively (Fig. 5). The bright emission at the fracture site [see also Fig. 4(b)] is somewhat surprising, as defected nanotubes are usually associated with reduced PL. Given the bright emission observed for air-suspended SWNT segments overhanging trenches, one might conclude that the "fracture site" in fact corresponds to a small "free-standing" piece of the SWNT lifted off the substrate by the AFM tip. However, this suggestion disagrees with the AFM images (obtained before PL measurements), which show no measurable height changes at the fracture sites (spatial resolution in z direction is ±0.15 nm). Also, such an interpretation cannot explain the very large blueshifts of $E_{11,22}$ observed for SWNT 1 at the point of maximum emission.

Another unusual PL feature observed for fractured SWNT 1 was emission intermittency (PL blinking) on the time scale of seconds. This was observed only at position −0.5 μm, i.e., close to the fracture site [Fig. 5(c)] and became more pronounced with increasing laser excitation power. PL blinking is typical for individual surfactant-coated SWNTs depos-

TABLE I. Average E_{11} and E_{22} energies, bandwidths [FWHM($E_{11,22}$)], and relative emission intensities for on-SiO$_2$ segments of SWNTs 1–4. The values in brackets indicate transition-energy shifts relative to air-suspended nanotube segments.

SWNT	(n,m) [a]	p [b]	E_{11} (meV)	E_{22} (meV)	FWHM E_{11} (meV)	FWHM E_{22} (meV)	Relative intensity[c]
1	(15,2)	1	787 (−11)	1526 (−7)	14	56	0.05–0.08
2	(13,2)	2	974 (−27)	1476 (−24)	19	47	0.06
3	(12,4)	2	956 (−7)	1498 (−5)	18.5	49	0.12
4	(16,2)[d]	2	803 (−23)		16.5		0.07

[a] (n,m) assignment is according to Ref. 9.

[b] $p=(n-m)\text{mod }3$ (see Note 26).

[c] Relative emission intensity of on-SiO$_2$ versus air-suspended SWNT segments.

[d] Tentative assignment (E_{22} energy profile is partly beyond our excitation range).

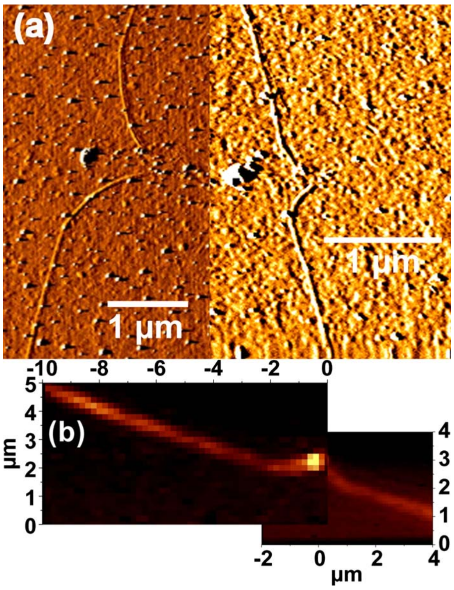

FIG. 4. (Color online) (a) AFM error signal images of SWNTs 1 and 2 (left and right panels, respectively) after fracturing by dragging an AFM tip across the nanotube (perpendicular to the cylinder axis); (b) PL image of SWNT 1 combined from two scans taken with pixel sizes of 0.2×0.2 and 0.1×0.1 μm^2 (left and right image fragments), respectively. This corresponds to the AFM image rotated counter clockwise by 90°. The bright emission spot can be related to the fracture site.

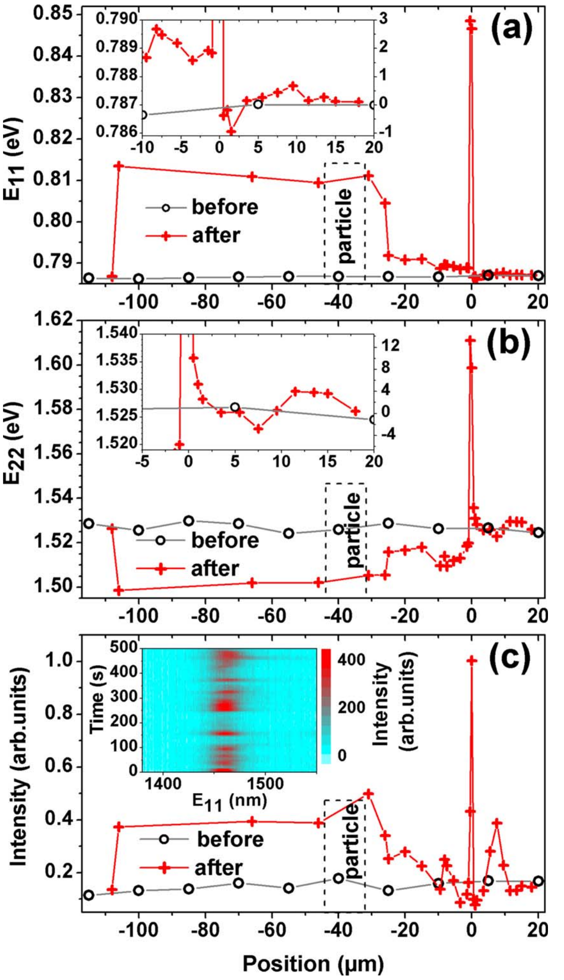

FIG. 5. (Color online) Length-profiles of PL peak energies (a) E_{11} and (b) E_{22} and (c) relative emission intensities for SWNT 1 before and after fracture (circles and crosses, respectively). Position 0 corresponds to the fracture site (see Fig. 4). The insets in (a) and (b) show enlarged profiles around this position. The PL localized at position −0.5 demonstrated fluctuations (blinking) with time as illustrated by the PL map inserted in (c) and combined from sequential PL spectra with color-coded PL intensity. The PL-intensity profile shows the average emission signal at this position.

ited onto various substrates from water-surfactant dispersions upon cooling to <25 K.[12] It has been attributed to photoinduced charge trapping (also) involving residual surfactant. In contrast, stable PL has usually been observed for CVD-grown surfactant-free SWNTs, both for air-suspended and on-SiO_2 segments. The present observation suggests that local emission intermittency at ambient temperature may be induced by significant structural damage, albeit of unclear molecular nature.

On either side of the fracture site (and relative to the unperturbed SWNT), the PL profiles show shifts of E_{11} and E_{22} energies which at the same positions have *different signs.* These shifts range up to 27 and −28 meV, respectively, and propagate along the nanotubes up to tens of micrometers away from the fracture site (Figs. 5 and S2). This can be explained in terms of manipulation-induced strain in SWNTs.[3,4,27–30] Dragging an AFM tip across an SWNT exerts "pushing" and "rolling" forces, thus generating axial strain σ and torsional (circumference) strain η.[3,4] The corresponding shift of the band-gap energy, ΔE_{11}, of a semiconducting SWNT can be approximated by[27–29]

$$\Delta E_{11} \approx -3\gamma_0(-1)^p[(1+\nu)\sigma\cos 3\theta + \eta\sin 3\theta], \qquad (1)$$

where $\gamma_0 \approx 2.7$ eV is the nearest-neighbor exchange integral, $\nu \approx 0.2$ is Poisson's ratio, and θ is the nanotube chiral angle. ΔE_{22} has similar magnitude and an analogous dependence on p and θ as does ΔE_{11} but has an opposite sign.[27–30] Compared to shifts induced by axial strain, the torsional strain contribution is usually small and has a shorter propagation length (see below). For SWNTs 1 and 2, which have small chiral angles, the effect of torsion is also further reduced by the factor of $\sin 3\theta$ contained in Eq. (1). Therefore, we attribute the major strain induced shifts in Figs. 4 and 3S to nanotube stretching.

Note that the shifts of E_{11} and E_{22} energies demonstrated by SWNT 1 also show opposite signs compared to the behavior observed for SWNT 2. This supports the (n,m) assignment of SWNT 1 and 2 to different nanotube families ($p=1$ and 2, respectively, Table I). SWNT 1 was additionally stretched between positions −25 and −105 μm via the force exerted by a ~13 μm large impurity particle. This was accidentally pushed up against the nanotube by the AFM cantilever (before the manipulation) between positions $-32\cdots-45$ μm as indicated in Fig. 5. An SEM image of the particle is shown in Fig. S3. This observation illustrates undesirable interference from impurity particles on the substrate surface. On the other hand, it suggests that strain may be intentionally generated (indirectly) via moving appropriate disklike microparticles with an AFM tip. This approach could allow large mechanical loads to be more steadily applied to SWNTs. It might also provide better control of torsional vs axial strain (see below).

Applying Eq. (1) to our measurements, we estimate axial strains of up to ~0.3% (particle-induced) and ~0.14% (residual after AFM manipulation) for SWNTs 1 and 2, respectively. Here, we assume that the nanotube interaction with the substrate can be neglected in the first approximation and Eq. (1) derived for free nanotubes can be applied. This assumption is justified, for instance, by similar dependences of PL shift vs axial strain observed for both air-suspended and matrix-entrapped individual nanotubes.[30–32] Interestingly, for SWNT 1 we observe that the nanoparticle-induced strain propagates for up to ~70 μm and then abruptly relaxes (at position −105 μm in Fig. 5). This is in contrast with the observations of Duan *et al.*[4] who reported gradual relaxation of axial strain over a length of ~350 μm. The latter relaxation scenario conceivably reflects a smoother surface with reduced numbers of "anchoring" impurities. For strained segments we found very little effect on the emission intensity,[33] only a small average increase in FWHM(E_{11}) by up to ~1–2 meV and no clear trend for FWHM(E_{22}) within the scatter of the experimental data.

All luminescent SWNT types are chiral, i.e., they can have either the left- or the right-handed mirror-image structure.[34] It is commonly accepted that as-prepared SWNT materials are racemic, i.e., contain equal amounts of left- and right-handed nanotubes.[35] However, the handedness of a *specific* individual nanotube remains difficult to determine because available atomically resolved imaging methods such as STM are inherently inefficient. We argue that a combination of PL microscopy and AFM manipulation can also provide the handedness of long luminescent nanotubes grown horizontally on appropriate substrates. Rolling such a chiral nanotube with an AFM tip (or with a "probe" microparticle) will generate a very specific pattern of torsional strain in the nanotube. The sign of the strain ε will depend both on the rolling vector and the nanotube handedness. Moreover, within the same chiral SWNT, the sign of the torsional strain will reverse across the manipulation (rolling) point. To understand this, one can consider a helical steel spring on a table, which is clamped at both ends as an analog to the chiral SWNT situation. If a lateral rolling force is applied to the spring at its middle point (perpendicular to its long axis), then the spring is coiled in one direction and unraveled in the other. Such a characteristic torsional strain pattern in an SWNT "nanospring" leads to characteristic E_{11} and E_{22} energy shifts according to Eq. (1). By taking into account the manipulation geometry (rolling vector) and (n,m) structure (from the PL measurements), the nanotube handedness can be determined from these shifts (and in particular their signs).

Note that gentle rolling of nanotubes is essential in the proposed method in order to keep the axial strain component and corresponding energy shifts in the PL spectra minimal.[36] Dragging SWNTs 1 and 2 with an AFM tip to their respective fracture points is apparently not optimal in this respect: the shifts of E_{11} and E_{22} in the PL profiles were dominated by the axial strain (stretching) component as discussed above. However, axial strain appears to be efficiently relaxed in one section of SWNT 1 as evidenced by the small energy shifts between positions 0.5 and 20 μm in Fig. 5. A closer inspection shows that ΔE_{11} is negative and ΔE_{22} is positive near the fracture site (at ~0.5–3 μm), whereas the opposite shifts, as expected for a stretched (15,2)-nanotube (SWNT 1), only develop further away from the fracture site. We interpret the former shifts as an indication of weak residual torsional strain of a compressive character ($\eta < 0$). Their disappearance within a few μm from the fracture can be rationalized in terms of a correspondingly short relaxation range of the torsional strain in on-SiO_2 nanotubes, in accordance with Raman results of Duan *et al.*[4] Torsional compression is observed below the fracture point as seen in Figs. 1 and 4 and for the manipulation (rolling) direction from left to right would correspond to a coiled right-handed spring. If this interpretation is correct, SWNT 1 is a right-handed (15,2) nanotube.

IV. SUMMARY

In summary, PL spectral imaging allows detailed characterization of long semiconducting SWNTs grown on silicon substrates. Brighter emission and blueshifts of the E_{11} and E_{22} energies are a hallmark of air-suspended nanotube segments relative to on-SiO_2 segments. For the latter, ~10–20 times weaker but still reliably measurable emission was observed. Acquiring PL maps at different locations along a nanotube (PL profiling) allows to check the uniformity of its (n,m) structure as well as to probe for the presence of mechanical strain. It can also reveal severe deformations of SWNTs. We found that nanotube fracture with an AFM tip can be accompanied by changes in the PL behavior of the fracture site compared to unperturbed regions. In particular, we observed localized PL blinking. Finally, a combination of atomic force and PL microscopy can allow measuring the characteristic shifts of E_{11} and E_{22} energies as a result of micromanipulation induced torsional strain. This opens the exciting possibility of determining the handedness of individual luminescent (=chiral) nanotubes by PL profiling after micromanipulation.

ACKNOWLEDGMENTS

This work was supported in part by the Deutsche Forschungsgemeinschaft (DFG) and by the Bundesministerium für Bildung und Forschung (BMBF).

*Corresponding author.
†lebedkin@int.fzk.de
‡manfred.kappes@chemie.uni-karlsruhe.de

[1] Y. Y. Zhang, J. Zhang, H. B. Son, J. Kong, and Z. F. Liu, J. Am. Chem. Soc. **127**, 17156 (2005).

[2] Z. Jin, H. B. Chu, J. Y. Wang, J. X. Hong, W. C. Tan, and Y. Li, Nano Lett. **7**, 2073 (2007).

[3] B. Gao, X. Duan, J. Zhang, T. Wu, H. Son, J. Kong, and Z. Liu, Nano Lett. **7**, 750 (2007).

[4] X. Duan, H. Son, B. Gao, J. Zhang, T. Wu, G. G. Samsonidze, M. S. Dresselhaus, Z. Liu, and J. Kong, Nano Lett. **7**, 2116 (2007).

[5] M. J. O'Connell, S. M. Bachilo, C. B. Huffman, V. C. Moore, M. S. Strano, E. H. Haroz, K. L. Rialon, P. J. Boul, W. H. Noon, C. Kittrell, J. P. Ma, R. H. Hauge, R. B. Weisman, and R. E. Smalley, Science **297**, 593 (2002).

[6] J. Lefebvre, P. Finnie, and Y. Homma, Phys. Rev. B **70**, 045419 (2004).

[7] D. Karaiskaj, C. Engtrakul, T. McDonald, M. J. Heben, and A. Mascarenhas, Phys. Rev. Lett. **96**, 106805 (2006).

[8] A. V. Naumov, S. M. Bachilo, D. A. Tsyboulski, and R. B. Weisman, Nano Lett. **8**, 1527 (2008).

[9] O. Kiowski, S. Lebedkin, F. Hennrich, S. Malik, H. Rosner, K. Arnold, C. Sürgers, and M. M. Kappes, Phys. Rev. B **75**, 075421 (2007).

[10] J. Lefebvre, D. G. Austing, J. Bond, and P. Finnie, Nano Lett. **6**, 1603 (2006).

[11] A. Hartschuh, H. N. Pedrosa, L. Novotny, and T. D. Krauss, Science **301**, 1354 (2003).

[12] H. Htoon, M. J. O'Connell, P. J. Cox, S. K. Doorn, and V. I. Klimov, Phys. Rev. Lett. **93**, 027401 (2004).

[13] O. Kiowski, S. Lebedkin, and M. M. Kappes, Phys. Status Solidi B **243**, 3122 (2006).

[14] S.-S. Jester, O. Kiowski, S. Lebedkin, F. Hennrich, R. Fischer, N. Stürzl, J. Hawecker, and M. M. Kappes, Phys. Status Solidi B **244**, 3973 (2007).

[15] See EPAPS Document No. E-PRBMDO-80-068931 for Supplementary Information: details of the AFM manipulation procedure; a typical microphotoluminescence map of an air-suspended nanotube segment (Fig. S1); profiles of the relative PL intensity and E_{11} and E_{22} transition energies as measured along the AFM-manipulated SWNT 2 (Fig. S2); an SEM image of the impurity particle pushed over SWNT 1 (Fig. S3). For more information on EPAPS, see http://www.aip.org/pubservs/epaps.html.

[16] Substrates with SWNTs were typically characterized by scanning electron microscopy after the AFM and PL experiments to avoid any possible damage of nanotubes by the electron beam. SEM images of nanotubes could then be readily correlated with the AFM and PL data due to markers on the substrates.

[17] Y.-Z. Ma, J. Stenger, J. Zimmermann, S. M. Bachilo, R. E. Smalley, R. B. Weisman, and G. R. Fleming, J. Chem. Phys. **120**, 3368 (2004).

[18] A. G. Petrov and S. V. Rotkin, Nano Lett. **3**, 701 (2003).

[19] V. Perebeinos, S. V. Rotkin, A. G. Petrov, and P. Avouris, Nano Lett. **9**, 312 (2009).

[20] S. K. Doorn, L. Zheng, M. J. O'Connell, Y. Zhu, S. Huang, and J. Liu, J. Phys. Chem. B **109**, 3751 (2005).

[21] The $E_{11,22}$ energies measured here for suspended nanotube segments in the nitrogen or argon atmosphere (see experiments) corresponded to those for nanotubes in vacuum (Ref. 9).

[22] T. Ando, J. Phys. Soc. Jpn. **66**, 1066 (1997).

[23] C. L. Kane and E. J. Mele, Phys. Rev. Lett. **90**, 207401 (2003).

[24] Y. Ohno, S. Iwasaki, Y. Murakami, S. Kishimoto, S. Maruyama, and T. Mizutani, Phys. Rev. B **73**, 235427 (2006).

[25] S. Chiashi, S. Watanabe, T. Hanashima, and Y. Homma, Nano Lett. **8**, 3097 (2008).

[26] $p=(n-m)\mathrm{mod}\,3=0,1,2$ Statistically, two thirds of nanotubes are semiconducting ($p=1,2$) and one third ($p=0$) is metallic.

[27] L. Yang and J. Han, Phys. Rev. Lett. **85**, 154 (2000).

[28] L. Yang, M. P. Anantram, J. Han, and J. P. Lu, Phys. Rev. B **60**, 13874 (1999).

[29] Yu. N. Gartstein, A. A. Zakhidov, and R. H. Baughman, Phys. Rev. B **68**, 115415 (2003).

[30] K. Arnold, S. Lebedkin, O. Kiowski, F. Hennrich, and M. M. Kappes, Nano Lett. **4**, 2349 (2004).

[31] H. Maki, T. Sato, and K. Ishibashi, Nano Lett. **7**, 890 (2007).

[32] T. K. Leeuw, D. A. Tsyboulski, P. N. Nikolaev, S. M. Bachilo, S. Arepalli, and R. B. Weisman, Nano Lett. **8**, 826 (2008).

[33] The increase in emission from the stretched segment of SWNT 1 between positions −30 and −105 μm in Fig. 5 is due to a Raman overtone, which overlaps with the strain-shifted E_{11}-E_{22} emission-excitation PL peak.

[34] The conventional (n,m) notation with positive indices n, m, and $n\geq m$ corresponds to right-handed SWNTs (following the usual definition for helical structures). Their left-handed counterparts can be indexed, for instance, as (m,n) nanotubes.

[35] G. Dukovic, M. Balaz, P. Doak, N. D. Berova, M. Zheng, R. S. Mclean, and L. E. Brus, J. Am. Chem. Soc. **128**, 9004 (2006).

[36] Note that axial and torsional strains are coupled in a chiral nanotube. However, axial strain generated by pure torsion and the corresponding E_{11} and E_{22} energy shifts are expected to be relatively small (see also Ref. 29).